Insights into Earth's Energy Imbalance from Multiple Sources

KEVIN E. TRENBERTH AND JOHN T. FASULLO

National Center for Atmospheric Research,[a] Boulder, Colorado

KARINA VON SCHUCKMANN

Mercator Océan, Ramonville St. Agne, France

LIJING CHENG

International Center for Climate and Environment Sciences, Institute of Atmospheric Physics, Chinese Academy of Sciences, Beijing, China

(Manuscript received 26 April 2016, in final form 24 June 2016)

ABSTRACT

The current Earth's energy imbalance (EEI) can best be estimated from changes in ocean heat content (OHC), complemented by top-of-atmosphere (TOA) radiation measurements and an assessment of the small non-ocean components. Sustained observations from the Argo array of autonomous profiling floats enable near-global estimates of OHC since 2005, which reveal considerable cancellation of variations in the upper 300 m. An analysis of the monthly contributions to EEI from non-ocean components (land and ice) using the Community Earth System Model (CESM) Large Ensemble reveals standard deviations of 0.3–0.4 W m^{-2} (global); largest values occur in August, but values are below 0.75 W m^{-2} greater than 95% of the time. Global standard deviations of EEI of 0.64 W m^{-2} based on top-of-atmosphere observations therefore substantially constrain ocean contributions, given by the tendencies of OHC. Instead, monthly standard deviations of many Argo-based OHC tendencies are 6–13 W m^{-2}, and nonphysical fluctuations are clearly evident. It is shown that an ocean reanalysis with multivariate dynamical data assimilation features much better agreement with TOA radiation, and 44% of the vertically integrated short-term OHC trend for 2005–14 of 0.8 ± 0.2 W m^{-2} (globally) occurs below 700-m depth. Largest warming occurs from 20° to 50°S, especially over the southern oceans, and near 40°N in all ocean analyses. The EEI is estimated to be 0.9 ± 0.3 W m^{-2} for 2005–14.

1. Introduction

Continually tracking Earth's energy imbalance (EEI) is a key to understanding climate variability and change and the immediate prospects for the future climate (Trenberth 2009; Trenberth et al. 2014; Hansen et al. 2011; von Schuckmann et al. 2016). Earth is warming mainly because of increases in carbon dioxide and other heat-trapping greenhouse gases in the atmosphere, and the disposition of that energy geographically and in depth in the ocean has substantial implications for understanding the climate system response. A first step to making good predictions is fully understanding where the excess heat is going in the Earth system, as this determines what its consequences are for the future climate and the oceans.

Recent estimates (e.g., IPCC 2013; Roemmich et al. 2015; Riser et al. 2016) suggest that some 93% of the EEI is going into the ocean, where it is manifested as changes in ocean heat content (OHC). The rest acts to melt Arctic sea ice and land ice, and warm the land and the atmosphere, and in the process alters the hydrological cycle and clouds, thereby providing feedback in various ways on the climate system (e.g., Trenberth et al. 2014, 2015a,b). However, attempts to track the flow of

Denotes Open Access content.

[a] The National Center for Atmospheric Research is sponsored by the National Science Foundation.

Corresponding author address: Kevin E. Trenberth, National Center for Atmospheric Research, P.O. Box 3000, Boulder, CO 80307.
E-mail: trenbert@ucar.edu

DOI: 10.1175/JCLI-D-16-0339.1

energy through the climate system and close Earth's energy budget have run into discrepancies, especially for changes from year to year and over a decade (Trenberth 2009; Trenberth and Fasullo 2010; Trenberth et al. 2014); and substantial differences exist among estimates of the energy flows (Hansen et al. 2011; Church et al. 2011; Riser et al. 2016; von Schuckmann et al. 2016).

These differences ought to be greatly reduced during the Argo era (Roemmich et al. 2009), which is the period after about 2005 when the global ocean has been adequately populated with over 3000 autonomous Argo floats to provide continuous coverage in most areas. The exceptions are marginal seas and coastal regions, and areas at high latitudes where seasonal sea ice plays a major role (von Schuckmann et al. 2016). Instrumented sea mammals also complement the Argo observations there (Roquet et al. 2013). Yet it is also readily evident from the products from several groups who have analyzed the available data into near-global gridded products that large differences remain on a monthly time scale, as we show here. Part of this continued discrepancy results from inherent high spatial structure associated with eddies in the ocean, which always leaves some doubt about the representative scales of any observation. But a major part relates to the mapping techniques used to infill gaps in space and time (Abraham et al. 2013; Boyer et al. 2016) and whether or not physical constraints are included.

Assimilating available data into a global ocean model using four-dimensional data assimilation most readily incorporates the latter. Not only does this utilize past observations by carrying the information forward in time in the model framework; it also allows all kinds of multivariate observations to be included, such as sea surface temperatures (space-based and in situ observations) and sea surface height (from altimetry) (e.g., Zuo et al. 2016). Some oceanographers have avoided this approach for fear of contamination of the resulting products by model biases, and indeed this concern is well justified, given the large model errors in simulations (e.g., Xue et al. 2012; Balmaseda et al. 2015; Palmer et al. 2016). Nevertheless, as shown here, the objective statistical analyses of available observations contain spurious variability.

In this paper, we explore the prospects for improving different OHC estimates by trying to achieve closure of the energy budget over time. Here we use top-of-atmosphere (TOA) radiation observations from Clouds and the Earth's Radiant Energy System (CERES) (Loeb et al. 2009) to constrain the EEI changes and thus the changes in OHC. The data and methods are given in section 2. Section 3 addresses how large the non-ocean component is. We use seven recent near-global (60°S–60°N) or global analyses of ocean heat content by different groups to present new results (section 4) on how the ocean is changing with depth and as a whole for the Argo era, post 2004. While the ocean is warming in all cases, the monthly variations are often quite different, and the rates of change of OHC imply changes that are unphysical. The new Ocean Reanalysis Pilot v5 (ORAP5) from the European Centre for Medium-Range Weather Forecasts (ECMWF) (Zuo et al. 2016) has a very different character that is more in step with the implied changes from CERES.

2. Data and methods

The various approaches to establishing the EEI are discussed in Trenberth (2009) and von Schuckmann et al. (2016). We use monthly TOA CERES Energy Balanced and Filled (EBAF) edition 2.8 radiation on $1° \times 1°$ grids (Loeb et al. 2009, 2012); see acknowledgments for data access. These, or an earlier generation, have been analyzed in many studies. Observations from CERES begin in March 2000, constituting a 15-yr-plus record. However, while the EEI at TOA net radiation R_T is too small to measure directly from satellite, instruments are far more stable than they are absolutely accurate, with calibration stability less than $0.3\,\mathrm{W\,m^{-2}\,decade^{-1}}$ (95% confidence) (Loeb et al. 2009), and hence there is considerable confidence in the changes from year to year. Therefore, the absolute value of R_T has to be established from an inventory of the energy and, in particular, estimates of mean ocean heat uptake (Trenberth 2009; Loeb et al. 2012).

A compilation of annual values of OHC for the top 700 m of the ocean from several sources was given by Balmaseda et al. (2013b) and updated in Trenberth et al. (2014). Xue et al. (2012) and Palmer et al. (2016) have examined results from dynamical models. The basic compilation of data comes from the World Ocean Database (Boyer et al. 2009), but different groups apply differing bias adjustments [such as to expendable bathythermograph (XBT) profiles] before the Argo period (Cheng et al. 2016). Quite different assumptions are also used on how to infill missing data (Abraham et al. 2013; Boyer et al. 2016), but it is less an issue after 2005.

The dataset availability is described in the acknowledgments. We use data from the surface to 2000-m depth updated from von Schuckmann and Le Traon (2011) (called KvS here). This approach is quite basic and simply averages all Argo data in boxes in order to detect large signals and potential data biases. Other Argo-based analyses are freely available gridded fields from the International Pacific Research Center (IPRC)

(http://apdrc.soest.hawaii.edu/projects/argo/); Scripps Institution of Oceanography (Roemmich and Gilson 2009); the Met Office EN4.1 (Good et al. 2013); and JAMSTEC77 (Hosoda et al. 2010), most of which are essentially from 60°N to 60°S, owing to data availability. EN4.1 is closer to global and includes a varying range of observations, since it dates back to 1900, although questions remain about quality south of 60°S. OHC from Cheng and Zhu (2016) for the upper 2000 m are also included, denoted as the Institute of Atmospheric Physics (IAP) data [see also Cheng et al. (2015)]. That work focused on the post-1940 period and applied new updated corrections for XBT profiles. It used an objective analysis method of ensemble optimum interpolation, but with phase 5 of the Coupled Model Intercomparison Project (CMIP5) model simulations providing error covariance and first guess; hence, that methodology lies between the simple objective analyses (i.e., EN4.1, IPRC, JAMSTEC77, and Scripps) and the data assimilation (i.e., ORA) methods.

Argo data have been analyzed by Roemmich and Gilson (2009, 2011), Willis et al. (2008, 2009), Roemmich et al. (2015), Riser et al. (2016), and Wijffels et al. (2016) and consist of global quality-controlled ocean temperature and salinity profiles and monthly objective analyses without the use of a dynamic model. Von Schuckmann et al. (2014) show how the omission of the Indonesian region in Argo analyses can miss as much as a 20% increase in global sea level. In contrast, Balmaseda et al. (2013a,b) use four-dimensional data assimilation of multivariate fields, including sea surface height from altimetry, with a full global ocean circulation model used to carry information from past observations forward in time. ORAP5 is a new prototype for an eddy-permitting ocean reanalysis (Zuo et al. 2016; Tietsche et al. 2016) following on from ORAS4, but with higher horizontal and vertical resolution and with an active sea ice model and sea ice assimilation. It has been run in reanalysis mode through 2013, with consistent data streams, quality control, and forcing fluxes. Therefore, it is mostly not affected by the discontinuities associated with operational running (as was the case of ORAS4 after 2010).

For ORAP5 we were provided with only the 0–700-m and 0–bottom OHC. Therefore, ORAP5 includes a contribution from 2000 m to the bottom, but in the absence of observations, the ocean there is heavily constrained, perhaps partly by the bias correction applied. The effect has been quantified (courtesy of M. Balmaseda), as discussed later in section 4, and it is indeed tiny.

In this paper we use analyses from 2005 through 2014, but the common period to all datasets is 2006–13, and the monthly means for this period are used to remove the annual cycle and generate anomalies. The focus of this paper is on monthly data, but we also use a "12-month running mean," which actually averages over 13 terms with the first and last weighted at 0.5 in order to preserve a centered result, to reduce the noise.

3. Constraining OHC: The non-ocean component

There is considerable month-to-month variability in the net radiation R_T at TOA associated with weather fluctuations (Trenberth et al. 2015a,b) so that the observed monthly anomaly standard deviation is 0.64 W m^{-2} for global means. For 2000–14, the global mean observed time series of R_T show no significant trend.

The CERES values depict the total EEI changes over time and therefore also include contributions from melting of Arctic sea ice and land ice, as well as small contributions from land and atmosphere. On average, those extras have been estimated to amount to about 0.07 W m^{-2} (Trenberth 2009; Hansen et al. 2011), but presumably they can be larger on monthly time scales (cf. Trenberth et al. 2015a). As estimated from observations in Trenberth and Fasullo (2013), the monthly standard deviation of continental mean net surface flux of energy is 2–3 W m^{-2}, and, presuming these are random from one continent to the next, it suggests an approximate monthly global anomaly of up to 0.3 W m^{-2} for land and ice components (allowing for land vs global area). The biggest component is likely to be anomalies of precipitation P and evapotranspiration E on land, and the $P - E$ component is estimated to be on the order of 0.05 mm day^{-1} over land or globally 0.4 W m^{-2} [based on the analyses of Trenberth and Fasullo (2013)]. These values should be interpreted as standard deviations and do not include seasonal variations, but they do allow for the area of land. However, the observational and reanalysis-based quantities contain errors, and the above are ballpark estimates only.

To quantify the magnitudes of the non-ocean component to R_T, we have used the NCAR Community Earth System Model (CESM1). The Community Earth System Model Large Ensemble (CESM-LE) (Kay et al. 2015) consists of a 30-member set of runs using coupled atmosphere, ocean, land, and sea ice model components. The simulations span from 1920 through 2100 using estimated observed historical (through 2005) and RCP8.5 projected external forcings from CMIP5. A detailed analysis of runs from 2000–14 is given in Trenberth et al. (2015b).

Here we have examined the global mean R_T as well as the global mean net surface energy fluxes F_s over the

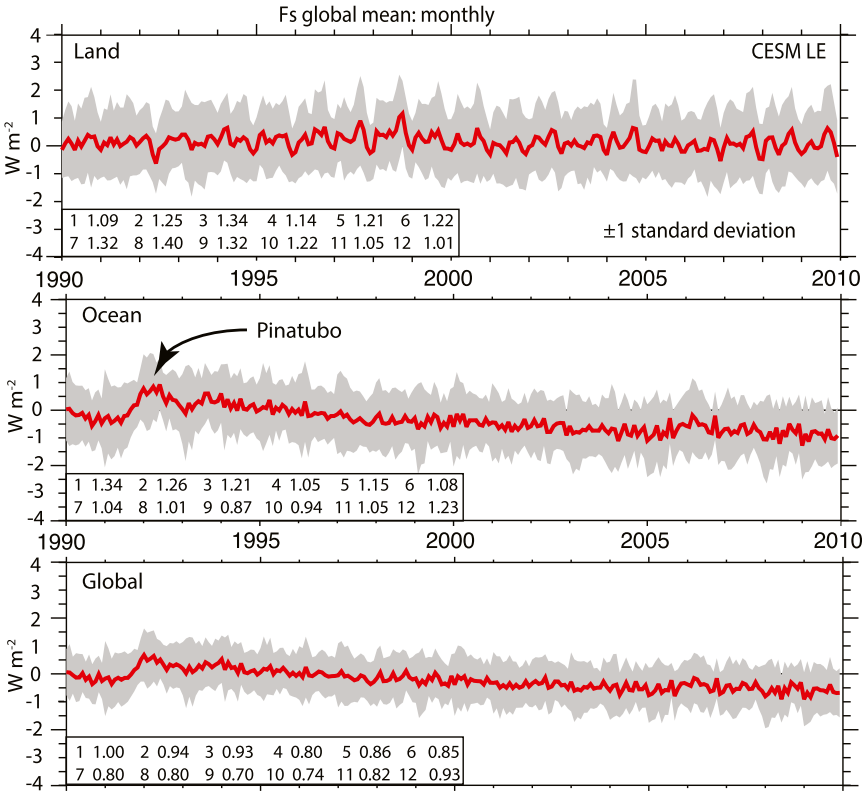

FIG. 1. From the CESM, based on 30 ensemble members, for each month the mean and ensemble standard deviation of the net surface flux of energy ($W m^{-2}$) for the (top) land, (middle) ocean, and (bottom) globe with the long-term mean removed. The gray shading shows plus and minus one standard deviation, and the mean annual cycle of the standard deviation is given in the lower inset for each of the 12 months. For this model and land–ocean mask, the land is 28% and the ocean 72% of the total, and these factors apply to the top two panels.

global oceans F_s^o and global land F_s^l, which sum to give R_T (Fig. 1). The atmospheric storage change term is in the noise level. Because there are 30 ensemble members, we can compute the mean fluxes in and out of land and ocean for any month along with a standard error, and we can also track this over time. As expected, there is a distinct annual cycle to F_s^l because most land is in the Northern Hemisphere.

The mean flux into the surface, area weighted to give the global contribution (i.e., the per square meters is global), in the model for this period is $0.1\,W m^{-2}$ for land and $0.8\,W m^{-2}$ into the ocean, with a global mean of $0.9\,W m^{-2}$. The model "land" includes inland seas and lakes. The main caveat to energy conservation over land (D. Lawrence 2016, personal communication) arises from water that enters the land from rain, which can be heated or cooled in the soil as the water flows through the soil column. At some point, that water may leave the column as subsurface runoff at a different temperature than it came in at, and the energy in rivers is not tracked. However, at the global scales, this imbalance is very small.

Results show that for 1990–2010 the average global land monthly standard deviation of F_s^l ranges from $1.01\,W m^{-2}$ in December to a maximum in northern summer in August of $1.40\,W m^{-2}$ (Fig. 1). Note that, for the global mean and the ocean, there are noticeable perturbations associated with the eruption of Mount Pinatubo in 1991. To allow for the area of land, the global contributions are 28% of the F_s^l or 72% of F_s^o. Hence, for F_s^l the global standard deviation contributions to R_T average 0.3 to a maximum of $0.4\,W m^{-2}$ in August. However, F_s^l and F_s^o are negatively correlated −0.09 in August (smaller in magnitude in other months) so that about 6% of the variance of F_s^l does not get reflected in R_T. Based on the model results, then, the non-ocean components can account for up to $0.76\,W m^{-2}$ (95% of the time) of R_T.

The net surface flux on land includes contributions from latent (precipitation, evapotranspiration) and sensible heat and radiation. The largest contributor is precipitation, and hence we have also computed the standard deviation of precipitation P on land in the same model runs (Fig. 2); and the overall standard deviation is

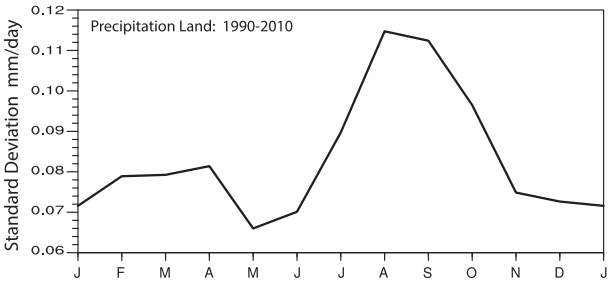

FIG. 2. Standard deviation as a function of time of year of global land precipitation in the CESM LE (mm day^{-1}).

0.0835 mm day^{-1}, equivalent to 0.68 W m^{-2} global contribution. It varies from a maximum in August of 0.115 mm day^{-1} to a low in May of 0.066 mm day^{-1} (Fig. 2). The highest values occur in August and September, as for F_s^l, and amount to 0.9 W m^{-2}. Because these are roughly double the global F_s^l net surface flux, they highlight that the evapotranspiration E is correlated with P, and the $P - E$ variance is much less than that for P alone, but also that these variations are likely the dominant contribution to the net surface flux anomalies.

In practice, these non-ocean components should be estimated on a monthly basis; but, for the current purpose, the values are small enough to constrain the OHC component, given the TOA flux.

4. OHC analyses

The OHC monthly variations and trends for 0–700 m and 0–2000 m after 2005 (Fig. 3) show a substantial upward trend but also reveal considerable fluctuations and discrepancies among the analyses from month to month, and with the Scripps data featuring a somewhat lower trend (Table 1). There is a marked contrast between the statistical time series and those from ORAP5. We have also included a time series of the integrated values of net radiation from CERES, where the base value for the mean was set at 0.8 W m^{-2}.

For ORAP5, the time series in Fig. 3 is 0–bottom, but the effect of the 2000 m to bottom layer is to increase the OHC at the end of 2013 relative to 2005 by 0.06×10^8 J m^{-2}, or, equivalently, the rate of warming for 2005–13 is greater by 0.015 W m^{-2} (global). For ORAP5, 56% of the linear trend in OHC occurs above 700 m and 44% below 700 m for 2005–13.

The CERES values are separately reproduced in the lowest panel (Fig. 3) along with 12-month running means of the ocean analyses and the unsmoothed ORAP5 series. This highlights the considerably different character of the monthly Argo time series and suggests that the subannual variations may be largely spurious. Here we also see a small jump in ORAP5 during 2008, which is spurious and arose from a change in the assimilated SST analysis (from a research to an operational product) (M. Balmaseda 2016, personal communication). The OHC 12-month running means have standard deviations reduced by about a factor of 5 (Table 1) and exhibit a character more similar to those of monthly CERES and ORAP5 time series. The lower panel of Fig. 3 also allows the low-frequency trends to be better compared, summarized in Table 1 as linear trends.

Breaking down the results by layer (Fig. 4) shows considerably better reproducibility from 0–100- and 100–300-m-depth layers among the analyses, with a large ENSO signal that strongly cancels between these two layers (Roemmich and Gilson 2011). The raggedness among the analyses increases with depth, and the trend stands out most strongly for the 700–2000-m layer. That layer is also where early values from Scripps differ substantially from the others, and hence their unduly low overall trend. Some features at depth, like the larger values toward the end of 2012 into 2013 have considerable reproducibility, which seems to improve after about 2008 as numbers of Argo observations increased somewhat (Cabanes et al. 2013, their Fig. 3).

The values in Figs. 3 and 4 are in units of joules per square meter, and the areas analyzed differ slightly but mostly pertain to 60°N–60°S. ORAP5 and EN4.1 contain global values, although there remains considerable uncertainty in polar regions in the absence of Argo observations there. The polar region time series are not regarded as definitive, as there is considerable sensitivity to steric versus mass partitioning of OHC (Zuo et al. 2016) that arises when altimetry data are assimilated without adequate temperature observations. Nevertheless, there appear to be increases of OHC in both Arctic and Subantarctic regions, accompanying the loss of Arctic sea ice (Tietsche et al. 2016) and relatively deep warm water undermining ice shelves around Antarctica (Jacobs et al. 2011; Bintanja et al. 2013), which are a clear manifestation of warming. For ORAP5, surface to bottom, the trend from 2005 to 2013 is 0.80 W m^{-2} globally versus 0.83 W m^{-2} for 60°N–60°S. Accordingly, for the analyses that have missing data, we have assumed that the missing areas of the ocean are changing at the same rate as the rest, and we infer the change in heat in the ocean by assuming the area is 0.362×10^{15} m^2. Hence, a change of -1.6 to $+1.6 \times 10^8$ J m^{-2} from the beginning of 2005 until the end of 2014 (Fig. 3) is equivalent to 0.71 W m^{-2} globally. For reference, 10^8 J m^{-2} is about 0.362×10^{23} J, and 10^{22} J yr^{-1} = 0.317 PW = 0.622 W m^{-2} globally.

These time series (Figs. 3, 4) suggest very different continuity and persistence from month to month among the products. This aspect can be examined from the rates of change of OHC (Fig. 5), which can be directly

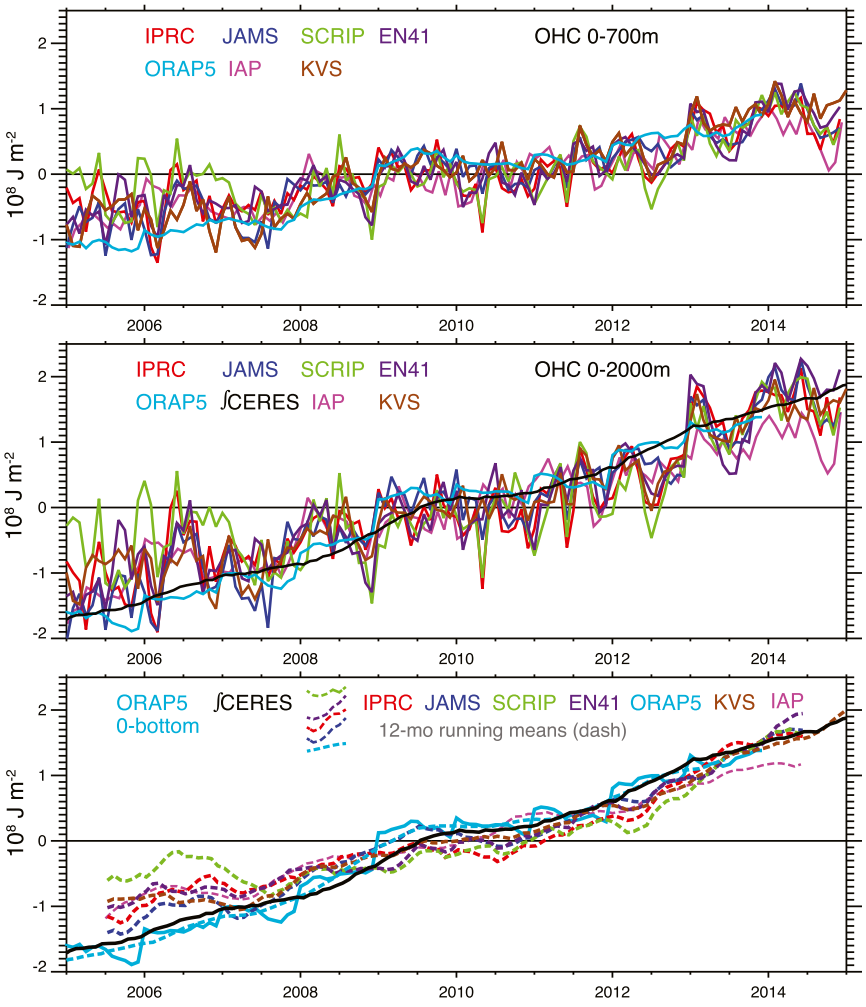

FIG. 3. Monthly OHC anomaly analyses for 2005–14 (10^8 J m^{-2}). Shown are IPRC, JAMSTEC, Scripps, EN4.1, IAP, KvS, and ORAP5. (top) The 0–700-m depth. (middle) The 0–2000-m depth; also included is the integrated CERES product. (bottom) The ORAP5 0–bottom time series and the CERES integral are reproduced to highlight the different character and are compared with 12-month running means of the other OHC time series (dashed).

compared with CERES values in watts per square meter globally (Table 1). Here the rates of change of OHC have been computed with a simple one-sided difference. The CERES values depict the total EEI changes over time and therefore include non-ocean contributions, but these are mostly less than 0.75 W m^{-2} (section 3). The OHC variations are also missing contributions from marginal seas and sea ice regions [assumed to change at the same rate as elsewhere, which is likely an underestimate (von Schuckmann et al. 2014)], as well as below 2000-m depth, although some studies have made adjustments for those (Roemmich et al. 2015).

The 0–2000-m OHC changes provide the most meaningful comparison with CERES, but the contributions to the total from each layer are also of interest. As noted above, the standard deviation of CERES values is 0.64 W m^{-2} (post 2005) (see Table 1). However, aside from ORAP5, the OHC fluctuations (Fig. 5) vary over a range of ±35 W m^{-2} and with a standard deviation of about 10–13 W m^{-2} for all Argo OHC datasets included in Table 1, thereby dwarfing the CERES variations. This suggests highly spurious and nonphysical OHC variations from month to month that are too large by a factor of about 15. This is true even for some features that are reproduced, suggesting common biases in the observation locations and their analysis.

Table 1 also shows the lag-1 month autocorrelation of the OHC itself. While these are dominated by trends, the Argo ocean analyses have values from 0.84 to 0.93, while the ORAP5 and CERES equivalent are much higher at >0.99. Computing tendencies is a form of high-pass filter and removes the trend effects. However, because

TABLE 1. For each of the given OHC near-global products, included are the following: autocorrelation (AC) at lag-1 month of OHC (or CERES equivalent); the monthly standard deviation (std dev) of the monthly rates of change of OHC ($W m^{-2}$); the corresponding standard deviation if smoothed with a 0.25 (1–2–1) smoother; standard deviation of the 12-month running mean; and the linear trend with 95% confidence limits ($W m^{-2}$) (global). All values are for 2005–14 and 0–2000-m depth, except ORAP5, which is through 2013 and 0–bottom (2% occurs below 2000 m).

Source	Lag-1 AC	Std dev	Std dev (1–2–1)	Std dev (12 month)	Trend
IPRC	0.89	11.8	6.0	1.31	0.56 ± 0.08
JAMSTEC	0.93	10.1	4.8	1.25	0.66 ± 0.07
Scripps	0.84	13.3	6.4	1.62	0.45 ± 0.10
EN4.1.1	0.88	8.9	4.7	1.11	0.53 ± 0.07
KvS	0.91	8.3	4.3	0.96	0.64 ± 0.06
IAP	0.93	6.4	3.6	0.91	0.56 ± 0.05
ORAP5	0.992	2.4	1.4	0.50	0.80 ± 0.04
CERES	0.999	0.64	0.44	0.28	

differentiation amplifies high-frequency noise, we have also computed the standard deviation of the OHC tendencies after smoothing with a 0.25 (1–2–1) binomial filter that knocks out 2-delta fluctuations entirely, but the resulting tendencies are still up to 5–8 $W m^{-2}$. Taking 12-month running means further reduces the noise to a more acceptable level, although still a factor of 4 too large. ORAP5 monthly values are also somewhat too large by a factor of 3 (Table 1), and some of this arises from the small inhomogeneity noted earlier in 2008.

The fluctuations of OHC over time can be better seen by taking zonal means over the oceans as a function of latitude (Fig. 6). Many large-scale changes over time are reproducible in all datasets, but the Argo analyses contain a lot of noise, thought to originate mainly from mesoscale eddies and details of the thermocline and its changes over time. These plots (Fig. 6) are all relative to a baseline annual mean for 2005, which was a relatively warm year for global mean surface temperature. Accordingly, there are some regions of cooling evident in the Northern Hemisphere in all analyses, especially around 55°N. The standout warming has occurred from 20° to 50°S and especially after 2011 from 40° to 50°S. There is also substantial warming near 40°N.

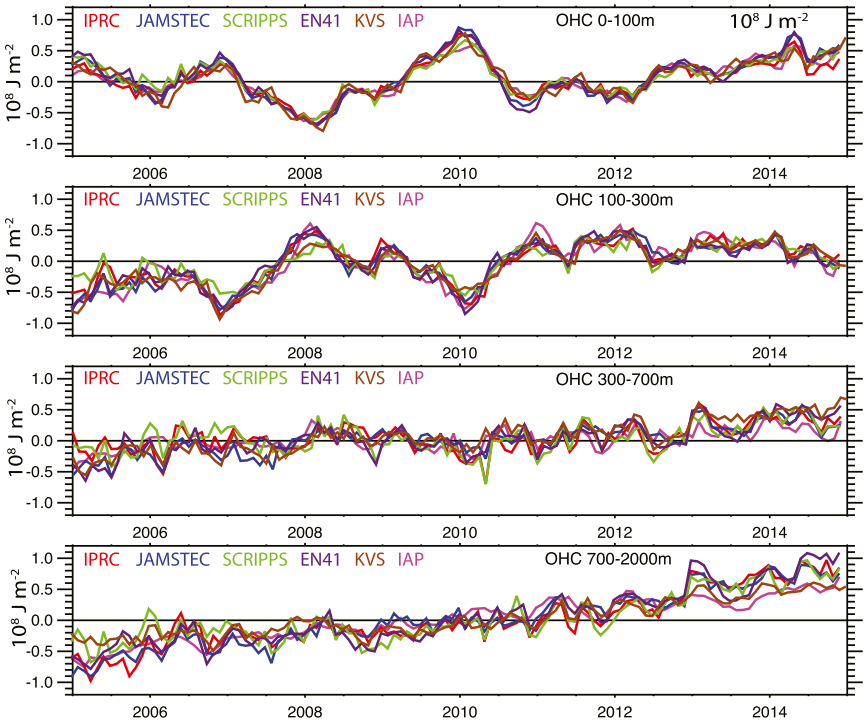

FIG. 4. Monthly OHC anomaly analyses for 2005–14 (10^8 J m^{-2}) for different layers. Shown are IPRC, JAMSTEC, Scripps, EN4.1, KvS, and IAP for (from top to bottom) 0–100, 100–300, 300–700, and 700–2000 m.

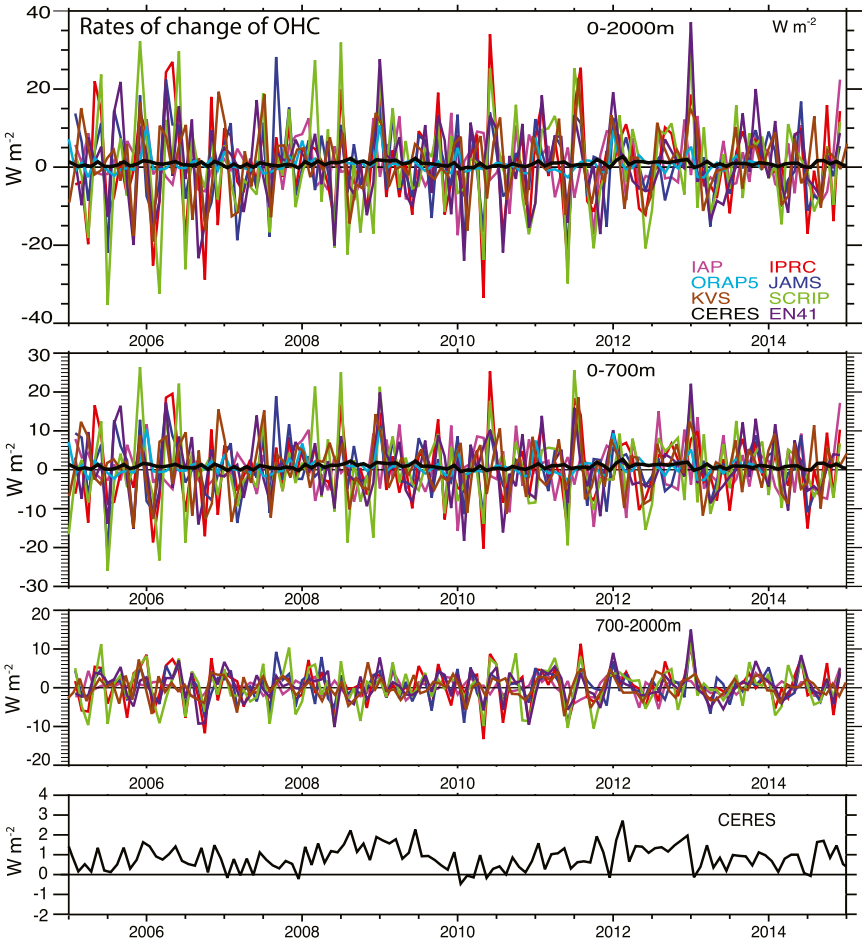

FIG. 5. Monthly rates of change of OHC for various layers ($W m^{-2}$) (global area): (top three panels) 0–2000 m, with CERES also included, 0–700 m, and 700–2000 m. (bottom) The CERES time series with an amplified vertical scale.

The warming can also be seen from linear trends between 2005 and either 2013 or 2014 (Fig. 7). Globally the linear trend of OHC warming ranges from 0.45 (Scripps) to 0.56 (IPRC), 0.66 (JAMSTEC), 0.53 (EN4.1), 0.56 (IAP), 0.64 (KvS), and 0.80 (ORAP5) $W m^{-2}$. The sampling fit of a linear trend has 95% confidence limits (Table 1) of close to 0.1 $W m^{-2}$, but there are also uncertainties related to the less than global sampling that improved after 2008, but with polar regions and marginal seas missing, leading us to assign an error bar for this period of 0.2 $W m^{-2}$.

5. Conclusions

For the period after 2005 when Argo floats populate the global ocean, there remain remarkably large differences between various ocean analyses for month-to-month variations. Here we examined six objectively analyzed ocean state products from 2005 to 2014 as well as one ocean reanalysis that has a dynamical model and data assimilation at its core. The focus is on OHC in the upper 2000 m of the ocean, which is presumed to encompass most of the variability and trends over time and therefore can be compared with an entirely different product of the energy imbalance at TOA. It should be possible to estimate the non-ocean component of the EEI to some level, and analysis of the CESM model results indicates that the magnitude of the fluctuations is less than 0.75 $W m^{-2}$ 95% of the time for monthly values, with a maximum in northern summer that appears to be mostly associated with anomalies in $E - P$ (e.g., drought).

For this period, the energy imbalance is estimated to be 0.9 ± 0.3 $W m^{-2}$. This includes small contributions from the non-ocean climate system components [0.04 $W m^{-2}$ for 2004–08 by Trenberth (2009), 0.07 $W m^{-2}$ in the 2000s increasing from about 0.03 $W m^{-2}$ in the 1990s by Hansen et al. (2011), and 0.03 $W m^{-2}$ from 1993 to 2008 by Church et al. (2011)] and from the deep ocean [0.07 $W m^{-2}$

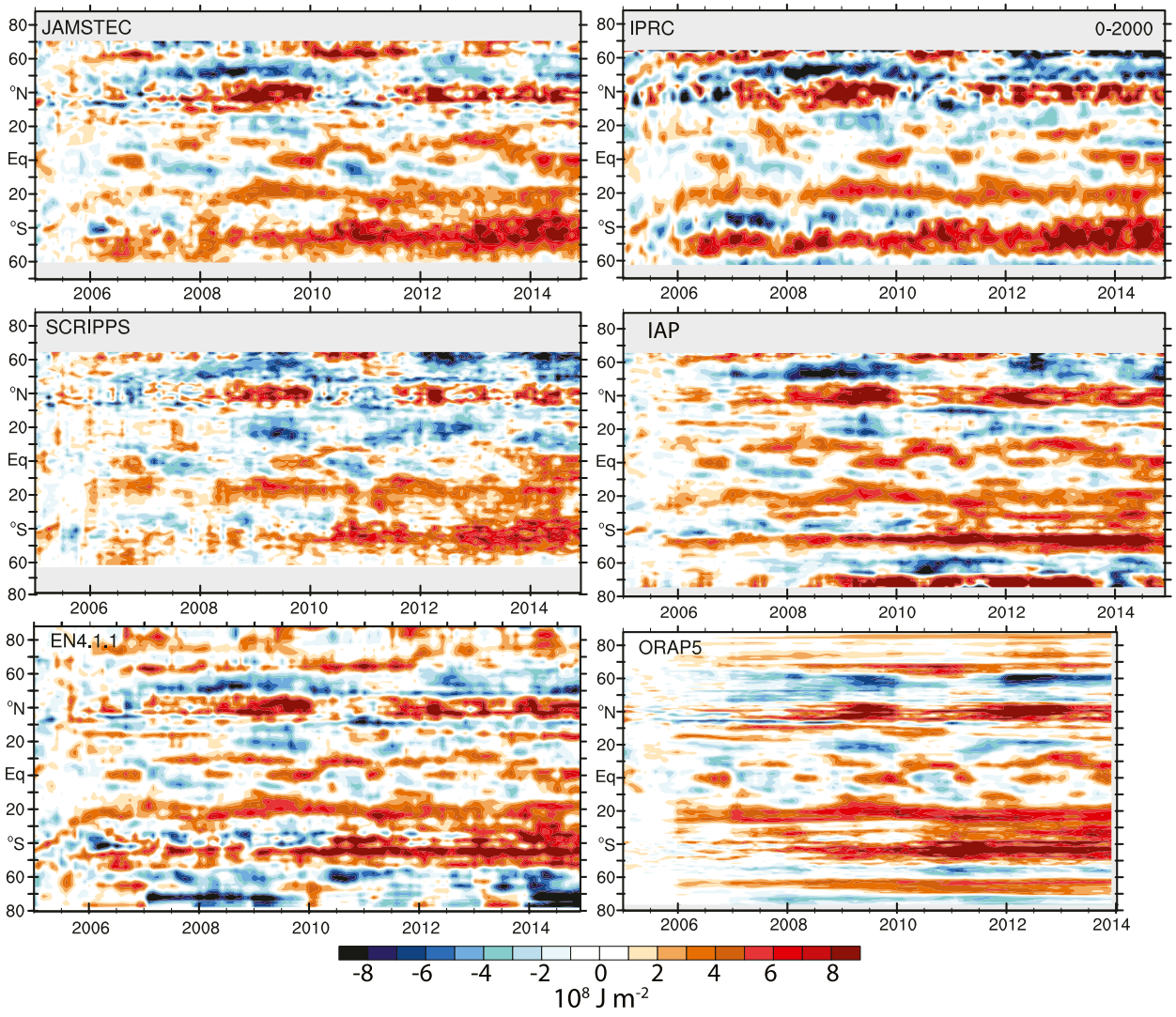

FIG. 6. Zonal mean OHC (10^8 J m^{-2}) over the oceans as a function of latitude and time for (left) JAMSTEC, Scripps, and EN4.1.1, and (right) IPRC, IAP, and ORAP5.

(Purkey and Johnson 2010)] (although ORAP5 included a 0.015 W m^{-2} contribution from below 2000 m). The global OHC component 0–2000 m is assessed to be 0.8 ± 0.2 W m^{-2}.

The total warming is substantially greater than the 0.4–0.6 W m^{-2} obtained by Roemmich et al. (2015) (here the Scripps dataset), owing to issues that are mainly apparent prior to 2008 between 700- and 2000-m depth. The largest warming has occurred over 20°–50°S, and especially over the southern oceans (Roemmich et al. 2015), which is reproducible among the various products, although with small-scale details varying considerably.

The focus here has been on examining monthly anomalies of the fields. Other studies introduced here focused on annual values where the results are more reasonable, but where the 12-month running means also have considerable discrepancies. Large variability is readily evident in OHC in all analyses that did not involve a dynamical model, and when the monthly tendency in OHC is computed and compared with CERES TOA measurements, the OHC month-to-month variability is shown to be spurious and nonphysical. Standard deviations of global monthly changes in OHC are about 12 W m^{-2} versus 0.64 W m^{-2} observed from CERES. In contrast, however, the OHC in an ocean reanalysis (as shown here for ORAP5) and its changes from month to month are much more realistic, suggesting either that there are shortcomings in the statistical procedures used to infill gaps in space and time in many of the ocean analyses or that the addition of sea surface

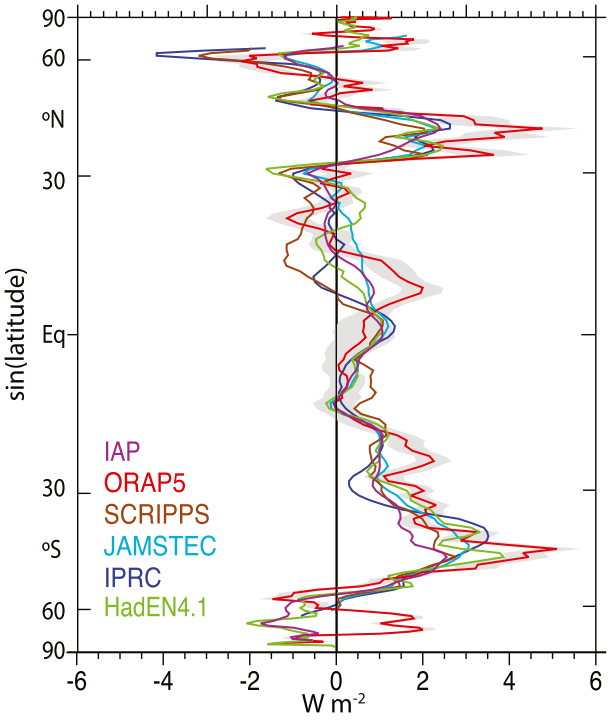

FIG. 7. Trends in the 0–2000-m zonal mean OHC ($W m^{-2}$) computed as linear trends between 2005 and 2013, where the area is ocean only as a function of latitude for IAP, ORAP5, Scripps, JAMSTEC, IPRC, and EN4.1.1. The coordinate is sine(latitude) to allow for the convergence of meridians. A 90% confidence limit has been placed on the ORAP5 curve.

height and SSTs makes a substantive difference. The ocean model in the reanalysis brings the information from past observations forward in time.

This kind of noise likely has major adverse effects on attempts to use the monthly analyses for predictive purposes or other applications, such as model validation. The noise is indicative of issues in infilling spatial and temporal gaps (Boyer et al. 2016) and has clearly led to underestimates of trends in OHC is some cases. For instance, in attempting to close the sea level rise budget, Rietbroek et al. (2016) determine that the steric rise in sea level since 2002 from residual computations is much greater than direct OHC analyses had suggested, but more in tune with values suggested here. As shown by Trenberth (2009), 1 mm yr^{-1} of sea level rise converts into a steric increase in global heat at a rate of 0.31–0.47 W m^{-2} above 700-m depth, or 0.68 W m^{-2} if all the warming is below 700-m depth, because of the different state temperatures with depth. Given that 44% of the warming is below 700-m depth, it is estimated that 1 mm yr^{-1} sea level rise is equivalent to about 0.52 W m^{-2} for the 2005–13 period. Hence, the steric component of sea level rise of 1.38 ± 0.16 mm yr^{-1} estimated by Rietbroek et al. (2016) is 0.72 ± 0.09 W m^{-2}, consistent with the values estimated here, but implying the need for revisions to the conclusions of Llovel et al. (2014).

We recommend that routine examination should be made of the rates of change of OHC in all analyses, and they should be constrained by TOA measurements of EEI along with estimates of other non-ocean components.

Acknowledgments. Many thanks to Magdalena Balmaseda and ECMWF for providing the ORAP5 dataset as well as information about it (Zuo et al. 2016). Thanks also to Yongxin Zhang for the information in Fig. 2. This research is partially sponsored by DOE Grant DE-SC0012711. The datasets are discussed in section 2, and most of those used are public domain. OHC datasets are listed on the Argo website (http://www.argo.ucsd.edu/Gridded_fields.html). Other datasets are available from the following websites: IPRC (http://apdrc.soest.hawaii.edu/projects/Argo/data/gridded/On_standard_levels/index-1.html); EN4.1.1 (http://hadobs.metoffice.com/en4/download.html); JAMSTEC (http://www.jamstec.go.jp/ARGO/argo_web/argo/?lang=en); and Scripps (http://sio-argo.ucsd.edu/RG_Climatology.html and ftp://kakapo.ucsd.edu/pub/gilson/argo_climatology/RG_ArgoClim_Temperature_2015.nc.gz). Datasets from Cheng and Zhu (2016) and von Schuckmann and Le Traon (2011) were provided by the lead authors. CERES data are available from the Langley Atmospheric Science Data Center (http://ceres.larc.nasa.gov/order_data.php).

REFERENCES

Abraham, J. P., and Coauthors, 2013: A review of global ocean temperature observations: Implications for ocean heat content estimates and climate change. *Rev. Geophys.*, **51**, 450–483, doi:10.1002/rog.20022.

Balmaseda, M. A., K. Mogensen, and A. T. Weaver, 2013a: Evaluation of the ECMWF Ocean Reanalysis ORAS4. *Quart. J. Roy. Meteor. Soc.*, **139**, 1132–1161, doi:10.1002/qj.2063.

——, K. E. Trenberth, and E. Källén, 2013b: Distinctive climate signals in reanalysis of global ocean heat content. *Geophys. Res. Lett.*, **40**, 1754–1759, doi:10.1002/grl.50382.

——, and Coauthors, 2015: The Ocean Reanalyses Intercomparison Project (ORA-IP). *J. Oper. Oceanogr.*, **8**, s80–s97, doi:10.1080/1755876X.2015.1022329.

Bintanja, R., G. J. van Oldenborgh, S. S. Drijfhout, B. Wouters, and C. A. Katsman, 2013: Important role for ocean warming and increased ice-shelf melt in Antarctic sea-ice expansion. *Nat. Geosci.*, **6**, 376–379, doi:10.1038/ngeo1767.

Boyer, T. P., and Coauthors, 2009: *World Ocean Database 2009*. NOAA Atlas NESDIS 66, 216 pp.

——, and Coauthors, 2016: Sensitivity of global ocean heat content estimates to mapping methods, XBT bias corrections, and baseline climatology. *J. Climate*, **29**, 4817–4842, doi:10.1175/JCLI-D-15-0801.1.

Cabanes, C., and Coauthors, 2013: The CORA dataset: Validation and diagnostics of in-situ ocean temperature and salinity measurements. *Ocean Sci.*, **9**, 1–18, doi:10.5194/os-9-1-2013.

Cheng, L., and J. Zhu, 2016: Benefits of CMIP5 multimodel ensemble in reconstructing historical ocean subsurface temperature variation. *J. Climate*, **29**, 5393–5416, doi:10.1175/JCLI-D-15-0730.1.

——, ——, and J. Abraham, 2015: Global upper ocean heat content estimation: Recent progress and the remaining challenges. *Atmos. Ocean. Sci. Lett.*, **8**, 333–338, doi:10.3878/AOSL20150031.

——, and Coauthors, 2016: XBT science: Assessment of instrumental biases and errors. *Bull. Amer. Meteor. Soc.*, **97**, 924–933, doi:10.1175/BAMS-D-15-00031.1.

Church, J. A., and Coauthors, 2011: Revisiting the Earth's sea-level and energy budgets from 1961 to 2008. *Geophys. Res. Lett.*, **38**, L18601, doi:10.1029/2011GL048794.

Good, S. A., M. J. Martin, and N. A. Rayner, 2013: EN4: Quality controlled ocean temperature and salinity profiles and monthly objective analyses with uncertainty estimates. *J. Geophys. Res.*, **118**, 6704–6716, doi:10.1002/2013JC009067.

Hansen, J., M. Sato, P. Kharecha, and K. von Schuckmann, 2011: Earth's energy imbalance and implications. *Atmos. Chem. Phys.*, **11**, 13 421–13 449, doi:10.5194/acp-11-13421-2011.

Hosoda, S., T. Ohira, K. Sato, and T. Suga, 2010: Improved description of global mixed-layer depth using Argo profiling floats. *J. Oceanogr.*, **66**, 773–787, doi:10.1007/s10872-010-0063-3.

IPCC, 2013: *Climate Change 2013: The Physical Science Basis*. Cambridge University Press, 1535 pp., doi:10.1017/CBO9781107415324.

Jacobs, S. S., A. Jenkins, C. F. Giulivi, and P. Dutrieux, 2011: Stronger ocean circulation and increased melting under Pine Island Glacier ice shelf. *Nat. Geosci.*, **4**, 519–523, doi:10.1038/ngeo1188.

Kay, J. E., and Coauthors, 2015: The Community Earth System Model (CESM) Large Ensemble Project: A community resource for studying climate change in the presence of climate variability. *Bull. Amer. Meteor. Soc.*, **96**, 1333–1349, doi:10.1175/BAMS-D-13-00255.1.

Llovel, W., J. K. Willis, F. K. Landerer, and I. Fukumori, 2014: Deep-ocean contribution to sea level and energy budget not detectable over the past decade. *Nat. Climate Change*, **4**, 1031–1035, doi:10.1038/nclimate2387.

Loeb, N. G., B. A. Wielicki, D. R. Doelling, G. L. Smith, D. F. Keyes, S. Kato, N. Manalo-Smith, and T. Wong, 2009: Toward optimal closure of the earth's top-of-atmosphere radiation budget. *J. Climate*, **22**, 748–766, doi:10.1175/2008JCLI2637.1.

——, J. M. Lyman, G. C. Johnson, R. P. Allan, D. R. Doelling, T. Wong, B. J. Soden, and G. L. Stephens, 2012: Observed changes in top-of-the-atmosphere radiation and upper-ocean heating consistent within uncertainty. *Nat. Geosci.*, **5**, 110–113, doi:10.1038/ngeo1375.

Palmer, M. D., and Coauthors, 2016: Ocean heat content variability and change in an ensemble of ocean reanalyses. *Climate Dyn.*, doi:10.1007/s00382-015-2801-0, in press.

Purkey, S., and G. Johnson, 2010: Warming of global abyssal and deep Southern Ocean waters between the 1990s and 2000s: Contributions to global heat and sea level rise budgets. *J. Climate*, **23**, 6336–6351, doi:10.1175/2010JCLI3682.1.

Rietbroek, R., S.-E. Brunnabend, J. Kusche, J. Schröter, and C. Dahle, 2016: Revisiting the contemporary sea-level budget on global and regional scales. *Proc. Natl. Acad. Sci. USA*, **113**, 1504–1509, doi:10.1073/pnas.1519132113.

Riser, S. C., and Coauthors, 2016: Fifteen years of ocean observations with the global Argo array. *Nat. Climate Change*, **6**, 145–150, doi:10.1038/nclimate2872.

Roemmich, D., and J. Gilson, 2009: The 2004–2008 mean and annual cycle of temperature, salinity, and steric height in the global ocean from the Argo Program. *Prog. Oceanogr.*, **82**, 81–100, doi:10.1016/j.pocean.2009.03.004.

——, and ——, 2011: The global ocean imprint of ENSO. *Geophys. Res. Lett.*, **38**, L13606, doi:10.1029/2011GL047992.

——, and Coauthors, 2009: Argo: The challenge of continuing 10 years of progress. *Oceanography*, **22**, 46–55, doi:10.5670/oceanog.2009.65.

——, J. Church, J. Gilson, D. Monselesan, P. Sutton, and S. Wijffels, 2015: Unabated planetary warming and its ocean structure since 2006. *Nat. Climate Change*, **5**, 240–245, doi:10.1038/nclimate2513.

Roquet, F., and Coauthors, 2013: Estimates of the Southern Ocean general circulation improved by animal-borne instruments. *Geophys. Res. Lett.*, **40**, 6176–6180, doi:10.1002/2013GL058304.

Tietsche, S., M. Balmaseda, H. Zuo, and K. Mogensen, 2016: Arctic sea ice in the global eddy-permitting ocean reanalysis ORAP5. *Climate Dyn.*, doi:10.1007/s00382-015-2673-3, in press.

Trenberth, K. E., 2009: An imperative for climate change planning: Tracking Earth's global energy. *Curr. Opin. Environ. Sustainability*, **1**, 19–27, doi:10.1016/j.cosust.2009.06.001.

——, and J. T. Fasullo, 2010: Tracking Earth's energy. *Science*, **328**, 316–317, doi:10.1126/science.1187272.

——, and ——, 2013: Regional energy and water cycles: Transports from ocean to land. *J. Climate*, **26**, 7837–7851, doi:10.1175/JCLI-D-13-00008.1.

——, ——, and M. A. Balmaseda, 2014: Earth's energy imbalance. *J. Climate*, **27**, 3129–3144, doi:10.1175/JCLI-D-13-00294.1.

——, Y. Zhang, J. T. Fasullo, and S. Taguchi, 2015a: Climate variability and relationships between top-of-atmosphere radiation and temperatures on Earth. *J. Geophys. Res. Atmos.*, **120**, 3642–3659, doi:10.1002/2014JD022887.

——, ——, and ——, 2015b: Relationships among top-of-atmosphere radiation and atmospheric state variables in observations and CESM. *J. Geophys. Res. Atmos.*, **120**, 10 074–10 090, doi:10.1002/2015JD023381.

von Schuckmann, K., and P.-Y. Le Traon, 2011: How well can we derive global ocean indicators from Argo data? *Ocean Sci.*, **7**, 783–791, doi:10.5194/os-7-783-2011.

——, J.-B. Sallée, D. Chambers, P.-Y. Le Traon, C. Cabanes, F. Gaillard, S. Speich, and M. Hamon, 2014: Consistency of the current global ocean observing systems from an Argo perspective. *Ocean Sci.*, **10**, 547–557, doi:10.5194/os-10-547-2014.

——, and Coauthors, 2016: An imperative to monitor Earth's energy imbalance. *Nat. Climate Change*, **6**, 138–144, doi:10.1038/nclimate2876.

Wijffels, S., D. Roemmich, D. Monselesan, J. Church, and J. Gilson, 2016: Ocean temperatures chronicle the ongoing warming of Earth. *Nat. Climate Change*, **6**, 116–118, doi:10.1038/nclimate2924.

Willis, J. K., D. P. Chambers, and R. S. Nerem, 2008: Assessing the globally averaged sea level budget on seasonal to interannual timescales. *J. Geophys. Res.*, **113**, C06015, doi:10.1029/2007JC004517.

——, J. M. Lyman, G. C. Johnson, and J. Gilson, 2009: In situ data biases and recent ocean heat content variability. *J. Atmos. Oceanic Technol.*, **26**, 846–852. doi:10.1175/2008JTECHO608.1.

Xue, Y., and Coauthors, 2012: A comparative analysis of upper-ocean heat content variability from an ensemble of operational ocean reanalyses. *J. Climate*, **25**, 6905–6929, doi:10.1175/JCLI-D-11-00542.1.

Zuo, H., M. A. Balmaseda, and K. Mogensen, 2016: The new eddy-permitting ORAP5 ocean reanalysis: Description, evaluation and uncertainties in climate signals. *Climate Dyn.*, doi:10.1007/s00382-015-2675-1, in press.